

Electron Clouds

G. Rumolo and G. Iadarola
CERN, Geneva, Switzerland

Abstract

The term ‘electron cloud’ refers to an accumulation of electrons inside the vacuum chamber of a particle accelerator, which is sufficiently strong to produce undesired effects on the accelerator operation, e.g., by causing beam loss, emittance growth, increase in the vacuum pressure, or unacceptable heat load on cold surfaces. Electrons in the beam chamber can primarily be generated by a number of processes, e.g., ionization of the residual gas. Their number, however, can exponentially increase via a beam-induced multipacting mechanism, which relies on acceleration of electrons in the field of the particle beam and efficient secondary emission from their impact on the chamber wall. Several machines running with high-intensity positively charged beams, made of trains of closely spaced bunches, suffer severe effects from electron clouds, and in some cases their performance is even limited by it. Techniques of electron cloud suppression or mitigation exist; the most popular ones are based on the reduction of the secondary electron yield of the chamber inner surfaces. This can be achieved passively through the so-called process of machine scrubbing, or actively by coating the inner pipe walls with appropriate low secondary electron yield materials.

Keywords

Collective effects; two-stream interactions; heat load; mitigation; scrubbing; coherent instabilities.

1 Introduction

In a particle accelerator, free electrons in the beam chambers can be generated by different mechanisms, such as ionization of the residual gas or photoemission from the chamber’s wall due to the synchrotron radiation emitted by the beam. When these electrons are accelerated in the electromagnetic field of the beam and reach the chamber walls, they may generate secondary electrons, in a number depending on the impact energy and on the secondary electron yield of the surface. When the accelerator is operated with closely spaced intense bunches of positively charged particles, and assuming that the secondary electron yield of the chamber’s inner walls is larger than one, this mechanism can drive an avalanche multiplication process of the electrons—known as multipacting—resulting in the formation of a so-called electron cloud in the chamber. Even accelerators operated with trains of negatively charged particle bunches can be affected by electron cloud formation, if the distance between subsequent bunches is such that the electrons emitted at the wall surface have enough time to move far into the vacuum chamber before they receive a strong repulsive kick back to the wall by the next coming bunch. The presence of a relatively large electron density in the beam pipe, as well as of a strong electron flux to the chamber’s wall, can limit the achievable performance of the accelerator through different detrimental effects, such as transverse beam instabilities, transverse emittance growth, particle losses, energy loss, vacuum degradation, and heating of the chamber’s surface. Electron cloud effects have been observed in several accelerators around the world, much more commonly in those operated with positively charged particles (e.g., positrons, protons, heavy ions), and are presently a major performance limitation for high-energy colliders, such as the Relativistic Heavy Ion Collider in the USA [1], the KEKB electron positron collider in Japan [2], the DAΦNE electron positron collider in Italy [3], and, more recently, the CERN LHC [4–7].

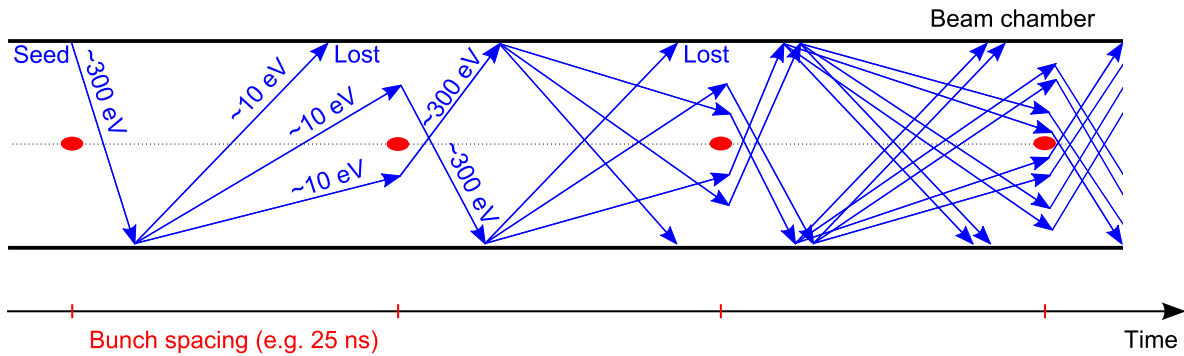


Fig. 1: Formation of an electron cloud in a particle accelerator (a similar sketch can be found in Ref. [8])

A qualitative sketch of the electron cloud build-up at a section of an accelerator operated with bunches of positively charged particles is given in Fig. 1 (see also Ref. [8]). The circulating beam particles can produce electrons through different mechanisms, e.g., ionization of the residual gas in the beam chamber or photoemission from the chamber's wall due to the synchrotron radiation emitted by the beam. These are called 'primary' or 'seed electrons'. Seed electrons are attracted by the passing particle bunch and can be accelerated to energies up to several hundred electronvolts. When an electron with this energy impacts the wall, 'secondary electrons' are likely to be emitted (the probability and efficiency of secondary emission for a certain energy of the incident electron are properties of the surface and also depend on its history). The secondaries have energies up to only few tens of electronvolts and, if they impact the wall with these energies, they are either absorbed or elastically reflected but cannot produce any secondary electrons. Conversely, if they survive until the passage of the following bunch they can in turn be accelerated, projected onto the wall, and produce secondary electrons.

This can trigger an avalanche multiplication effect, which builds up the electron cloud during the passage of an entire bunch train. Although this picture is instructive and represents a possible process leading to an avalanche creation of electrons inside the vacuum chamber, it is important to highlight that this is not a unique resonance condition occurring for a narrow range of the beam parameters and chamber radius. In reality, several different conditions for multipacting can be found, e.g., based on the acceleration of the electrons through multiple bunches or hitting a cyclotron resonance with an external magnetic field.

Section 2 will introduce the different phenomena involved in the formation of an electron cloud; Section 3 will then describe the main features of the electron cloud build-up mechanism. Finally, Sections 4 and 5 will review how the presence of an electron cloud in the beam chambers can affect the performances of a particle accelerator and what countermeasures can be taken.

2 Electron cloud build-up

2.1 Primary electrons

The circulating beam particles can produce electrons through different mechanisms, in particular:

- **ionization of the residual gas in the beam chamber:** this mechanism is always present and is responsible for a production rate of electron-ion pairs proportional to the vacuum pressure and to the ionization cross-section for the colliding particles' species and their energies. These electrons are therefore generated within the volume swept by the beam and must be initialized within the beam cross-section in numerical simulations. Usually, the ionization of the residual gas occurs through a scattering process; however, the rate of electrons produced can become much higher if the electric field of the beam is above the threshold for direct field ionization, i.e., for very intense and bright beams, as might be required for future lepton colliders;

- **photoemission from the chamber’s wall:** this mechanism applies to high-energy particle beams (usually for leptons, but this applies also to protons in the LHC), which emit a significant amount of synchrotron radiation with frequencies above the work function of the metal of which the inner wall of the beam chamber is made. The photons of the synchrotron radiation will therefore produce electrons (‘photoelectrons’) with a certain production efficiency (‘photoemission yield’). The photoelectrons are generated at the chamber wall surface, usually with a large fraction concentrated within the small cone of direct incidence of the synchrotron radiation against the chamber wall and the rest distributed around the remaining part of the wall, according to distributions depending on the chamber geometry;
- **beam particle loss at the inner wall of the beam chamber:** this mechanism depends on the loss rate and the electron emission rate for the grazing incidence of high-energy particles. However, in standard operation, losses are usually very low by design in particle accelerators, except in collimators or aperture restrictions, where they are controlled, so the previous two mechanisms are generally dominant as sources of primary electrons.

The electrons produced through these mechanisms are called ‘primary’ or ‘seed’ electrons, which are usually produced in sufficiently small amount that they would not affect the accelerator or the beam if their number was not exponentially amplified by the mechanism described in the next subsection. Only the photoelectrons, which can be produced in large amounts, owing to the large number of photons generated by high-energy particles circulating in a ring, have the potential to accumulate to the point of affecting the beam, even in the absence of any amplification mechanism. In any case, primary electrons interact electromagnetically with the passing particle bunch and can be accelerated to energies up to several hundred electronvolts.

2.2 Secondary electron emission

The secondary electron emission process can be described through the secondary electron yield of the surface, which is defined as the ratio between the electron current impinging the wall and the corresponding emitted electron current, and is a function of the energy of the impacting electrons:

$$\delta(E) = \frac{I_{\text{emit}}}{I_{\text{imp}}(E)}. \quad (1)$$

A typical secondary electron yield curve is presented in Fig. 2. Following the approach presented in Refs. [9–13], this quantity can in turn be decomposed into two main components:

$$\delta(E) = \delta_{\text{elas}}(E) + \delta_{\text{true}}(E), \quad (2)$$

where $\delta_{\text{elas}}(E)$ and $\delta_{\text{true}}(E)$ represent the electrons that are elastically reflected by the surface and the so-called ‘true secondaries’, respectively. The dependence of the two components on the energy of the impacting electrons is shown by the green and red curve in Fig. 2. The close-up displayed in the right-hand plot of Fig. 2 shows that elastic reflection of electrons impinging the wall plays a significant role only for very low energies (typically below a few tens of electronvolts) and causes electrons in this range of energies to have a much higher probability of survival on impact. This mechanism is not at all negligible in terms of electron cloud build-up, as it obviously helps to increase the speed of electron accumulation.

We will call δ_{max} the maximum of the secondary electron yield curve, which occurs for a certain energy of the incident electron E_{max} . Both these parameters are strongly dependent on surface material, roughness, and history and play a key role in the electron cloud build-up, as will be discussed in Section 2.3. In the following, δ_{max} will be often referred to simply as the ‘secondary electron yield parameter’. A typical energy distribution of the true secondary electrons is shown in Fig. 3. True secondary electrons are emitted with a cosine angular distribution with respect to the direction normal to the surface and their energy spectrum is well fitted by a ‘log-normal’ distribution.

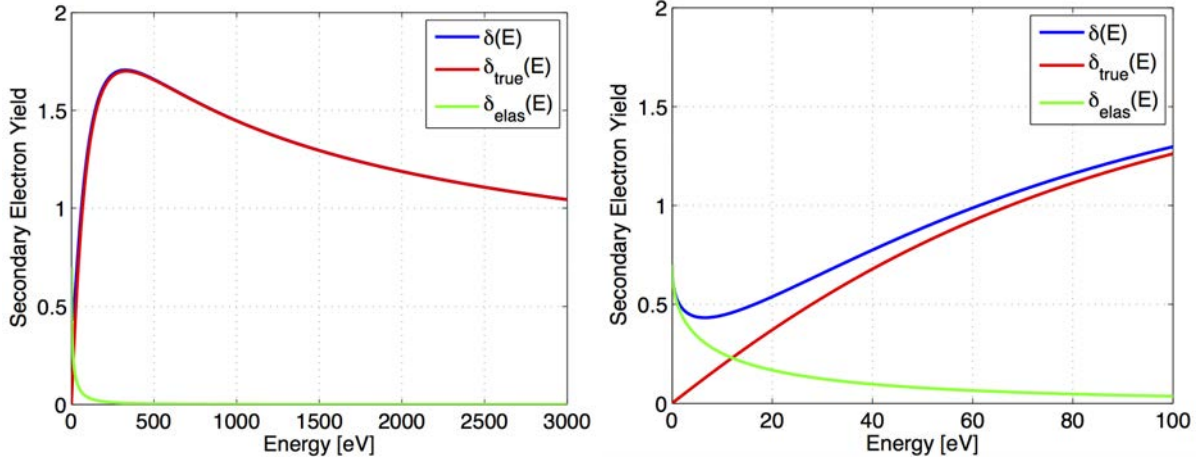


Fig. 2: Left-hand side: secondary electron yield curve for $\delta_{\max} = 1.7$; elastic component $\delta_{\text{elas}}(E)$, ‘true secondary’ component $\delta_{\text{true}}(E)$, and total $\delta(E)$. Right-hand side: close-up of low-energy region.

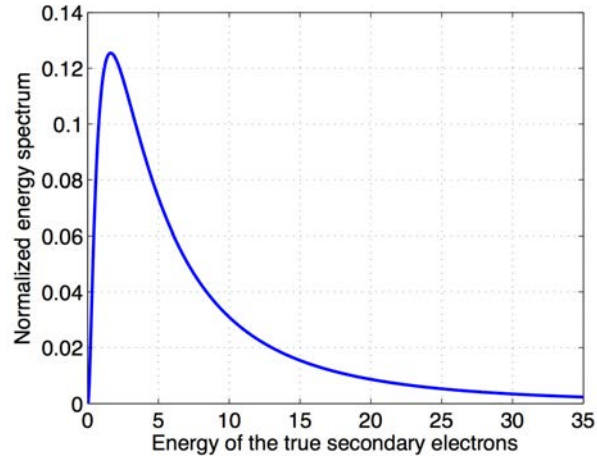


Fig. 3: Energy distribution of true secondary electrons

2.3 Electron cloud build-up mechanism

Let us consider a train of uniformly spaced bunches passing at a certain section of an accelerator, which does not contain any electron before the passage of the first bunch. Let n_0 be the number of primary electrons generated by a single-bunch passage and n_i the number of electrons in the chamber at the instant t_i right before the passage of the i th bunch. We can define $\delta_{\text{eff},i}$ such that

$$n_{i+1} = \delta_{\text{eff},i} n_i + n_0, \quad (3)$$

where $\delta_{\text{eff},i} n_i$ is the number of electrons generated by the interaction of the electron cloud with the chamber’s wall (such a quantity can also be negative, when the wall acts as a net electron absorber).

The quantity $\delta_{\text{eff},i}$ can be directly related to the secondary electron yield of the chamber’s surface $\delta(E)$ and to the energy spectrum of the impacting electrons, since we can write

$$n_{i+1} = n_i + \int_0^\infty \int_{t_i}^{t_{i+1}} \Phi(E, t) (\delta(E) - 1) dt dE + n_0, \quad (4)$$

where

$$\Phi(E, t) = \oint n(\vec{r}, E, t) \vec{v} \cdot dS \quad (5)$$

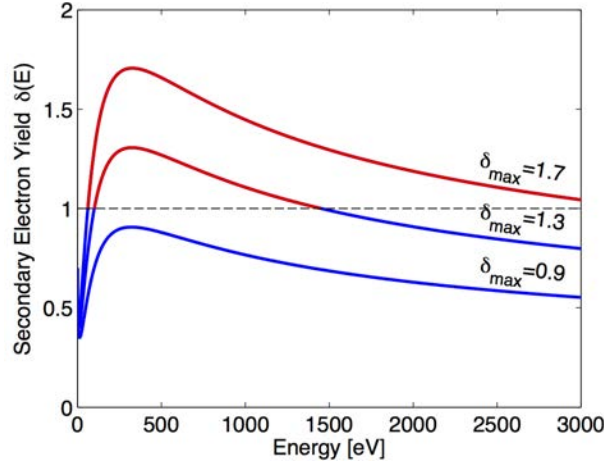


Fig. 4: Secondary electron yield curve for different values of δ_{\max} . Values for which the material behaves as electron absorber or emitter are plotted in blue and red, respectively.

is the instantaneous energy spectrum of the electrons impinging the wall. If we define the normalized energy spectrum for the the i th bunch passage as

$$\phi_i(E) = \frac{1}{n_i} \int_{t_i}^{t_{i+1}} \Phi(E, t) dt, \quad (6)$$

we can rewrite Eq. (4) as

$$n_{i+1} = n_i \left(1 + \int_0^{\infty} \phi_i(E) (\delta(E) - 1) dE \right) + n_0 \quad (7)$$

and, comparing this with Eq. (3), we obtain

$$\delta_{\text{eff}, i} = 1 + \int_0^{\infty} \phi_i(E) (\delta(E) - 1) dE. \quad (8)$$

The meaning of this equation is quite intuitive: the secondary electron yield curve can be divided into two regions, one in which $\delta(E) < 1$ and the wall acts as an electron absorber, and the other in which $\delta(E) > 1$ and the wall acts as an electron emitter. The two regions are shown in blue and red, respectively, in Fig. 4, for different values of δ_{\max} . Looking at Eq. (8), we observe that, if the electron flux $\phi_i(E)$ mainly overlaps the $\delta(E) < 1$ region, the integral is negative, $\delta_{\text{eff}, i} < 1$, and the chamber's wall behaves like a net absorber. Conversely, if $\phi_i(E)$ mainly overlaps the $\delta(E) > 1$ region, the integral is positive, $\delta_{\text{eff}, i} > 1$, and the chamber's wall behaves like a net emitter.

If the electrons do not influence each other's trajectories, which means that the Coulomb forces between them are negligible, then we can assume that $\phi_i(E)$ does not depend on the bunch index:

$$\phi_i(E) = \phi(E), \quad (9)$$

hence the same holds for $\delta_{\text{eff}, i}$:

$$\delta_{\text{eff}, i} = \delta_{\text{eff}}. \quad (10)$$

In these conditions, by recursively applying Eq. (3) we find:

$$n_i = n_0 \sum_{k=1}^i \delta_{\text{eff}}^k = n_0 \frac{1 - \delta_{\text{eff}}^i}{1 - \delta_{\text{eff}}}. \quad (11)$$

From this expression, we can recognize two different regimes. When $\delta_{\text{eff}} < 1$, we observe that, for sufficiently large i , n_i tends to the constant value:

$$n_i \simeq \frac{n_0}{1 - \delta_{\text{eff}}}, \quad (12)$$

which is essentially an equilibrium condition between primary electron production and electron absorption at the chamber's wall. We will therefore call this condition the *seed accumulation regime*.

When $\delta_{\text{eff}} > 1$, we observe an exponential growth of the number of electrons in the chamber, i.e., for sufficiently large i :

$$n_i \simeq n_0 \frac{\delta_{\text{eff}}^i}{\delta_{\text{eff}} - 1}, \quad (13)$$

which is indeed an avalanche multiplication of the electrons driven by the secondary emission. We will therefore call this condition the *multipacting regime*.

In the seed accumulation regime, a significant amount of electrons can be accumulated only if the primary electron production mechanisms are very strong, as can be the case for synchrotron radiation in a high-energy lepton machine, while, typically for hadron accelerators, sizeable electron cloud effects are only observed in the multipacting regime.

Equation (13) seems to suggest that the number of electrons can increase indefinitely. In fact, other mechanisms intervene to limit the number of electrons. To explore the validity of this simple model, we used the PyECLOUD code [14] to simulate the electron cloud build-up in the very simple case of a cylindrical chamber (radius 22 mm, i.e., the horizontal size of the LHC arc beams screen) without any externally applied magnetic field, with nominal LHC bunch parameters, and a uniform train of 25 ns spaced bunches. For the analysis of these results, it is also useful to introduce a few other quantities, namely the total electron flux on the chamber's wall,

$$F_i = \int_0^\infty \int_{t_i}^{t_{i+1}} \Phi(E, t) dt dE, \quad (14)$$

and the fractions of the impacting electrons that lie in the region of the secondary electron yield curve, where the wall acts as an electron absorber or electron emitter, respectively:

$$F_{\text{absor}, i} = \int_{\{E: \delta(E) < 1\}} \int_{t_i}^{t_{i+1}} \Phi(E, t) dt dE, \quad (15a)$$

$$F_{\text{emit}, i} = \int_{\{E: \delta(E) > 1\}} \int_{t_i}^{t_{i+1}} \Phi(E, t) dt dE. \quad (15b)$$

The simulation results for the case $\delta_{\text{max}} = 1.1$ are shown in Fig. 5. In particular, the blue curve in the top plot shows the evolution of n_i . In the middle plot we compare two ways of estimating the $\delta_{\text{eff}, i}$ coefficients from the simulation results, i.e., using both the recursive formula, Eq. (3), and simulated bunch-by-bunch electron spectra to evaluate the integral in Eq. (8). The two estimates are very consistent, showing that the angular dependence of the secondary electron yield, which is included in the simulation but not in the estimate of Eq. (8), is, in this case, negligible. The bottom plot shows, finally, the evolution of the coefficients $F_{\text{absor}, i}$ and $F_{\text{emit}, i}$, as defined in Eq. (15). The energy spectrum as defined in Eq. (6) is shown in the bottom plot of Fig. 6, while the top plot shows the secondary electron yield curve using the same x -axis range. Figure 6 shows that the energy spectrum $\phi_i(E)$ is the same all along the simulation (i.e., the condition of Eq. (9) is fulfilled) and lies mainly in the energy region for which the wall behaves as an electron absorber.

For the case of $\delta_{\text{max}} = 1.75$, the results are presented in Figs. 7 and 8. In these plots we can recognize two different stages, one going from the first passage up to around the 45th, and the second

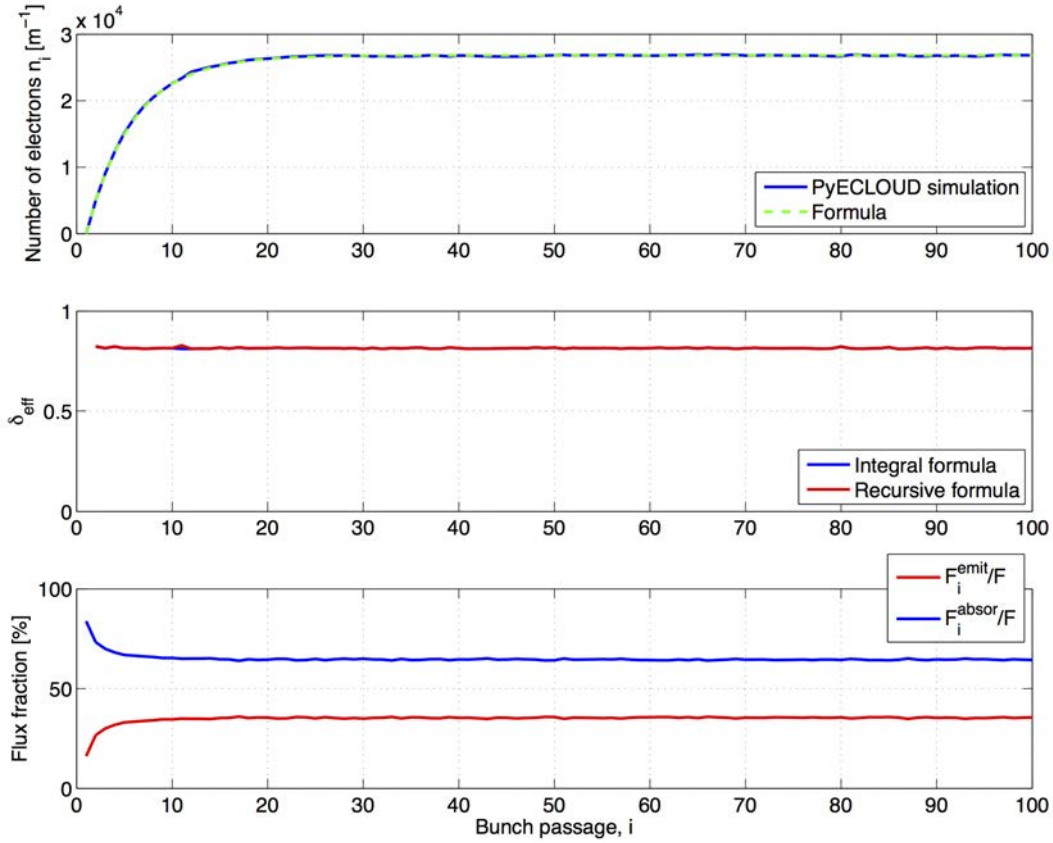


Fig. 5: Simulated electron cloud build-up for cylindrical tube of radius 22 mm, with nominal LHC bunch parameters, a uniform train of 25 ns spaced bunches, and $\delta_{\max} = 1.1$. Top: number of electrons before each bunch passage (blue, directly from simulation; dashed green, estimated from Eq. (11)). Centre: δ_{eff} (both from the integral formula, Eq. (8), and the recursive formula, Eq. (3)). Bottom: fractions of the electron energy spectrum falling in the absorber or emitter regions of the secondary electron yield curve.

from that point onward. In the first stage, the condition of Eq. (9) is verified and $\delta_{\text{eff}, i}$ is greater than one, which means that we are in the multipacting regime. Indeed, the energy spectrum $\phi_i(E)$ lies mainly in the energy region where the wall behaves like a net electron emitter, as confirmed by Figs. 7 (bottom) and 8. In this case Eq. (11) predicts an exponential increase in the number of electrons, which is exactly what is observed Fig. 7 (top).

Later on, we observe that the evolution of n_i deviates from the expected exponential increase and finally ‘saturates’ to a constant value, which is larger than the equilibrium value reached in the seed accumulation regime by several orders of magnitude (compare Figs. 5 and 7). By looking at Fig. 8, we observe that during this transition the condition of Eq. (9) is no longer fulfilled, since one can notice a strong increase in the number of electrons hitting the wall with extremely low energy (< 10 eV). We also observe that the electron flux becomes dominated by the fraction lying in the net absorber region (see Fig. 7, bottom) and that the effect of this change in the electron spectrum is that the parameter $\delta_{\text{eff}, i}$ reduces to one (see Fig. 7, middle).

The reason for this change can be understood by considering the fact that most true secondary electrons are emitted with energies of the order of a few electronvolts (see Fig. 3), and therefore, if they impact on the wall before being accelerated by a bunch passage, they have a high chance of being absorbed (the wall acts as net absorber for these energies, see Fig. 8, top). Figure 9 shows how the electron density and the electrostatic potential evolve during the build-up (all plots correspond to snapshots taken immediately before the passage of the corresponding bunch).

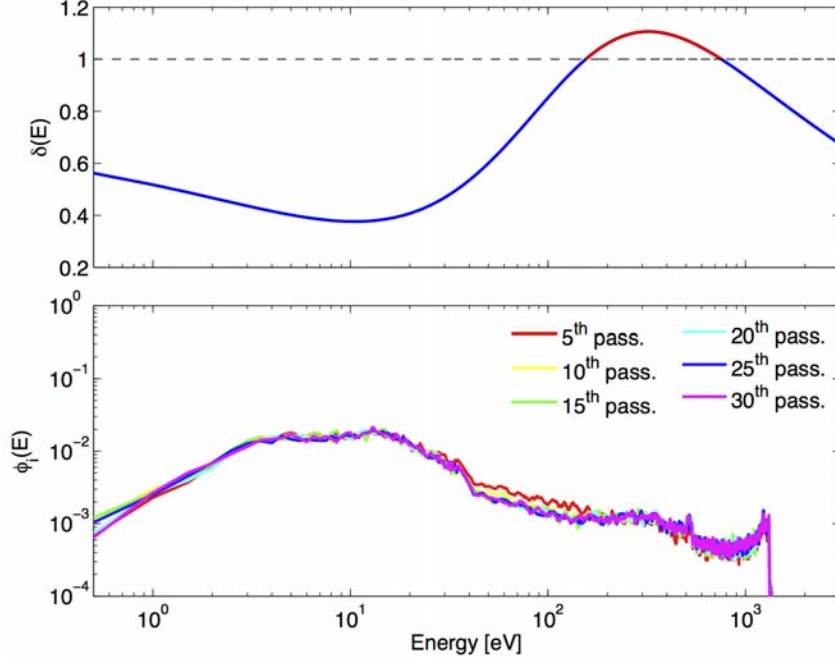


Fig. 6: Top: secondary electron yield curve. Bottom: energy spectrum $\phi_i(E)$ for different bunch passages

During the first stages, the electron density is quite modest, and, as a result, the electrostatic potential in the chamber (with respect to the wall) is less than 1 eV. In these conditions, most of the true secondaries are practically free to move in the chamber. Owing to their initial velocity, they drift towards the centre and have a high chance of avoiding impact on the wall before the next bunch passage.

As the electron density in the chamber increases, so also does the electrostatic potential, which means that the forces due to ‘space charge’ effects within the electron cloud itself become increasingly stronger. Around the 45th bunch passage, the true secondaries emitted by the wall see a potential barrier comparable to their kinetic energy and therefore tend to be confined in a region close to the chamber’s wall. As a consequence, the electron density assumes an annular shape (see Fig. 9) and the probability that low-energy electrons reach the wall before the next passage strongly increases.

This causes the change in the energy spectrum observed in Fig. 8 towards an equilibrium condition such that:

$$\int_0^{\infty} \phi_i(E) (\delta(E) - 1) dE = 0. \quad (16)$$

Here, electron emission and absorption at the wall perfectly balance one another and therefore $\delta_{\text{eff}, i} = 1$ (see Eq. (8)).

Figure 10 shows how the maximum number of electrons in the chamber and δ_{eff} in the first stage of the build-up simulation (before space charge effects become significant) depend on the secondary electron yield parameter δ_{max} . The value of δ_{max} for which $\delta_{\text{eff}} = 1$ is called the *multipacting threshold* and separates the seed accumulation and the multipacting regimes. The multipacting threshold can be easily recognized also by the number of electrons in the the beam chamber (see Fig. 10, top), since around this point an increase of several orders of magnitude is observed with respect to the seed accumulation regime. This kind of dependence is also observed for many other quantities related to the electron cloud in the chamber, e.g., the electron flux onto the wall, the electron density at the beam position, and the energy deposition onto the wall. Typically, if δ_{max} is below the multipacting threshold and therefore no avalanche multiplication occurs, the electron cloud tends to be harmless for the machine performance, unless very strong seeding mechanisms are present, as previously discussed.

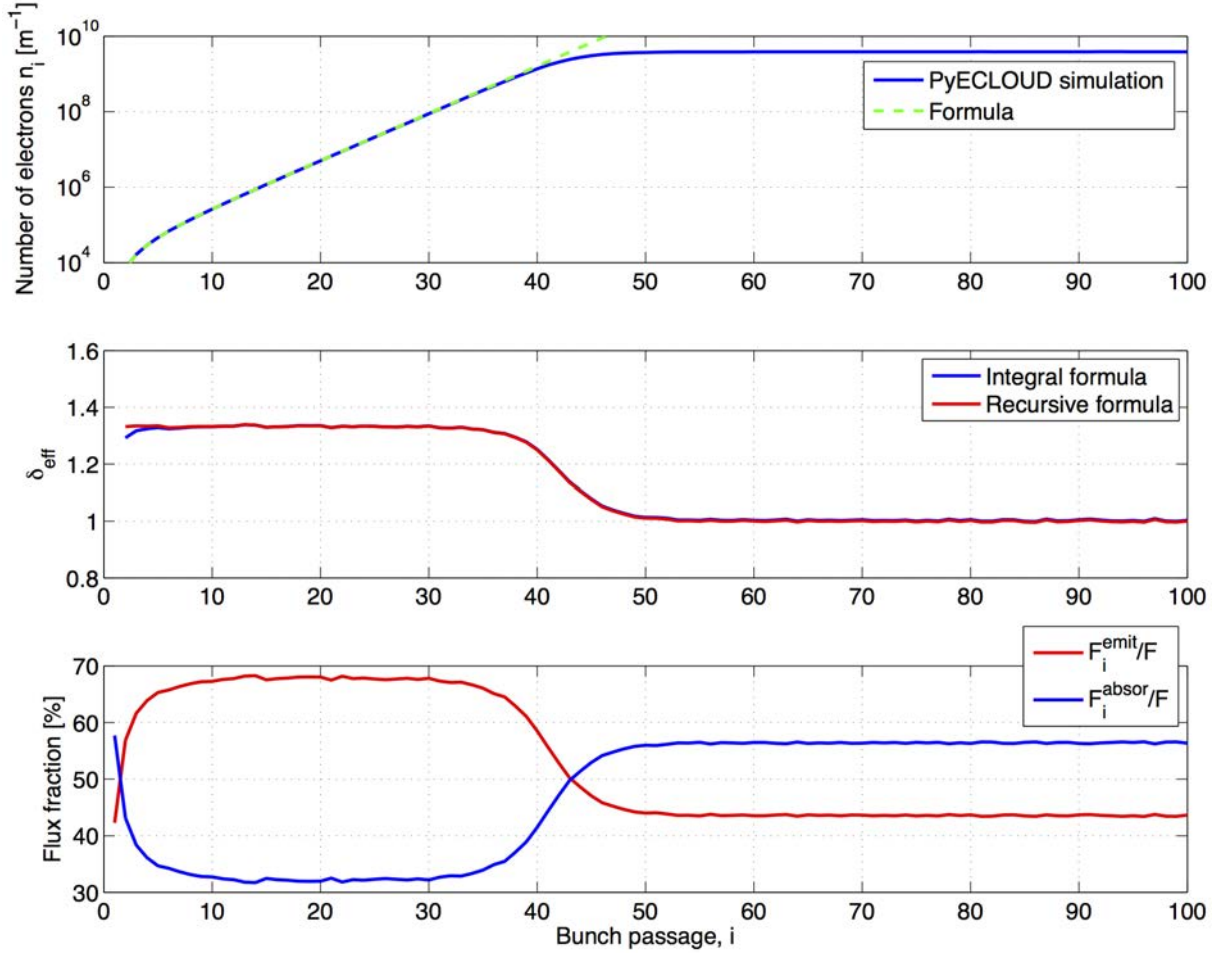


Fig. 7: Simulated electron cloud build-up for $\delta_{\max} = 1.75$. Top: number of electrons before each bunch passage (blue, directly from simulation; dashed green, estimated from Eq. (11)). Centre: δ_{eff} (both from the integral formula, Eq. (8), and the recursive formula, Eq. (3)). Bottom: fractions of the electron energy spectrum falling in the absorber or emitter regions of the secondary electron yield curve.

2.4 Effect of externally applied magnetic fields

The features of the electron cloud build-up are strongly influenced by externally applied magnetic fields, like those present in bending and focusing magnets of a particle accelerator.

It is simple to prove [15] that a non-relativistic electron moving in a uniform magnetic field of magnitude B (as for example in the case of a bending magnet) follows a helicoidal trajectory around the field lines. In a typical electron cloud build-up, the total kinetic energy of an electron is typically not larger than 2 keV (see, for example, the energy spectra in Figs. 6 and 8), which implies that the cyclotron radius never exceeds a few millimetres. This means that the electrons are practically constrained to move around the field lines. Electrons trapped by different field lines will receive different kicks from the passing bunches according to their horizontal positions, giving rise to different efficiencies for the multipacting process. If the energies to which the electrons are accelerated to the wall span from a value above E_{\max} at the centre of the chamber and a value below E_{\max} at the sides of the chamber, there will be two horizontal positions (symmetrical with respect to the chamber axis), for which the production of secondary electrons is maximally efficient. This generates the characteristic two-stripe pattern of the electron density in the chamber, like the one shown in Fig. 11 (left-hand side).

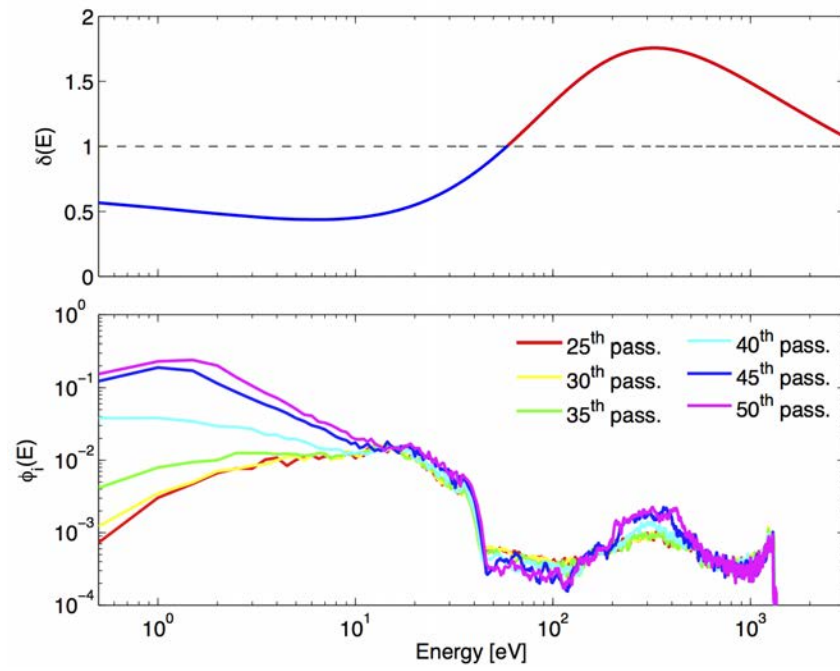


Fig. 8: Top: secondary electron yield curve. Bottom: energy spectrum $\phi_i(E)$ for different bunch passages

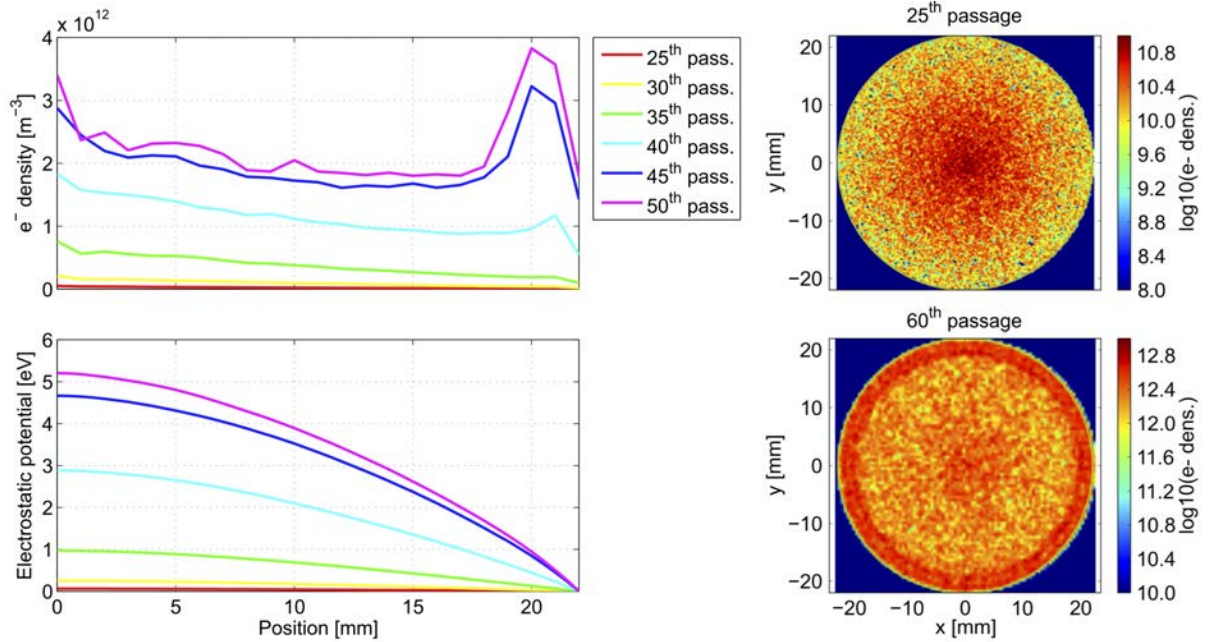


Fig. 9: Simulated electron cloud build-up for $\delta_{\max} = 1.75$. Left-hand side: electron density and electrostatic potential as a function of the distance from the centre and of the bunch passage. Right-hand side: snapshots of the electron density in the chamber, one taken immediately before a bunch passage during the exponential increase (top) and one taken immediately before a bunch passage during the saturation phase (bottom).

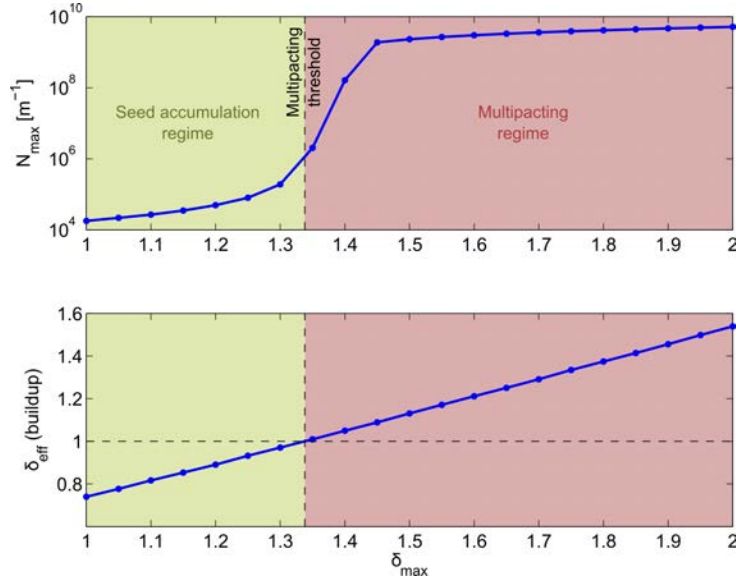


Fig. 10: Maximum number of electrons in the chamber and δ_{eff} coefficient as a function of the secondary electron yield parameter.

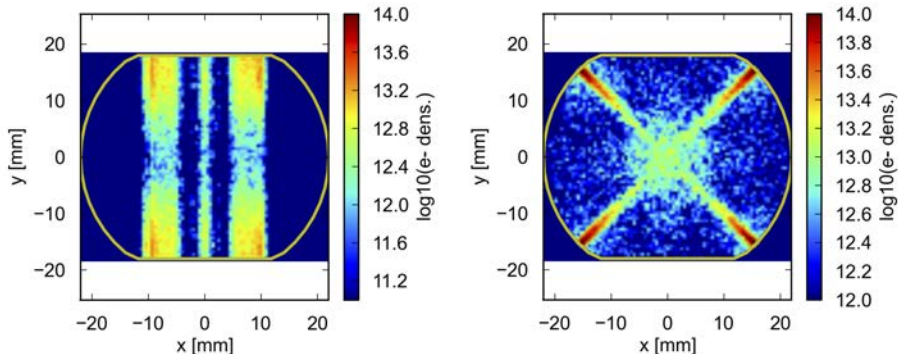


Fig. 11: Snapshots of the electron cloud density in a dipole (left-hand side) and a quadrupole (right-hand side) magnet of the LHC.

Similar effects are also observed in quadrupole magnets. For example, with the chamber and beam parameters of LHC, the electron density shows an X-like shape as shown in Fig. 11 (b). In the case of quadrupoles, the presence of a magnetic field gradient can also trigger electron-trapping mechanisms, which can make the electron cloud build-up even more severe by helping electron survival between the passage of successive bunches [16].

3 Impact of electron cloud effects on the accelerator’s performances

The presence of an electron cloud in the beam chamber of a particle accelerator can limit its achievable performance through different effects, which will be briefly reviewed next. In general, the effects of the electron cloud in a particle accelerator can be classified as:

- **global:** the electron cloud is present in a large fraction of the machine and can significantly influence the beam dynamics;
- **local:** the electron cloud is only generated in certain machine elements (owing to their geometry or wall properties). Its impact on the beam dynamics is usually negligible, but it can nevertheless be responsible for local (detrimental) phenomena.

3.1 Impact on beam dynamics: coherent and incoherent effects

When the electron cloud covers a significant fraction of a machine, the integrated effect of its electric forces on the particle beam affects the collective beam motion, leading to a coherent tune shift, as well as to the onset of different types of transverse coherent instability above a certain electron density threshold. When a particle beam suffers a transverse instability (horizontal or vertical), the beam signal seen on a beam position monitor increases exponentially and the unstable motion eventually leads to emittance blow-up or fast beam loss. Electron cloud effects can, obviously, only appear in a machine operating with long trains of bunches, because, as was explained in the previous sections, the electron cloud only builds up and reaches saturation after several bunch passages. Despite this, both coupled-bunch and single-bunch phenomena (typically affecting only the last bunches in a long train) have been observed in running machines and were studied in the past, showing that the electron cloud can indeed be the source of unconventional wake fields, which affect the beam dynamics in a similar fashion as an impedance source. A multibunch dipole-mode instability was observed at the KEK Photon Factory on positron beam operation, and was subsequently explained as an effect of the variation in the electron cloud centroid position induced by an offset bunch, which can feed into the motion of subsequent bunches in an unstable loop [17]. More studies on this subject were carried out for the Beijing Electron Positron Collider and for the PEP-II B factory. Coupled-bunch instabilities in the horizontal plane were also observed at CERN, first at the Super Proton Synchrotron with LHC-type beams [18], and then at the Proton Synchrotron in the last phase of production of the LHC-type beams [19]. They were also recorded at the LHC during the first injections of trains of 48 bunches of a 25 ns spaced beam [20]. Fortunately, owing to their coupled-bunch nature, these instabilities can usually be damped by a transverse feedback system without posing excessively stringent requirements on its bandwidth.

With a similar mechanism, however, an electron cloud inside the beam pipe can also be the origin of a short-range wake field for a bunch that goes through it, giving rise to head–tail coupling and single-bunch instabilities. Since this mechanism relies on the pre-existence of an electron cloud when the bunch arrives, it can obviously only affect the bunches at the tail of a long train, such that the electron cloud has formed with the passage of the preceding bunches. Assuming that the bunch goes into the electron cloud with its head slightly offset, a global net force will act on the electrons around the head centroid position and consequently an accumulation of electrons will take place in that region. The newly reconfigured electron distribution will thus kick the following bunch particles towards the higher-density region. The motion of the head will therefore be transmitted and potentially amplified at the tail of the bunch. The tail deflection will then increase over successive turns and will eventually transfer back to the head, thanks to the longitudinal mixing given by the synchrotron motion (after a few synchrotron periods). This head–tail coupling mechanism naturally follows the oscillation of the electrons in the bunch potential and therefore the oscillation frequency of the associated wake can be roughly expressed as

$$\omega_{ey(x)} = \sqrt{\frac{Nr_e c^2}{2\sigma_{y(x)}\sigma_z(\sigma_x + \sigma_y)}}. \quad (17)$$

In this equation, N is the number of positively charged particles in the bunch, $\sigma_{x,y,z}$ its r.m.s. sizes in the three directions, and r_e represents the classical electron radius. The frequency given by Eq. (17) can quickly reach the gigahertz range and above, especially for high-intensity or brightness, high-energy beams made of trains of short bunches. Owing to the important high-frequency content, the conventional transverse feedback systems are usually incapable of controlling this type of electron cloud induced instability. One has to rely instead on altering the head–tail phasing through high-chromaticity settings, or on Landau damping [21] using octupole magnets. Solutions of this type, however, typically come at the expense of transverse emittance preservation and beam lifetime [22,23]. The single-bunch instability due to the electron cloud, observed in the Super Proton Synchrotron and in the LHC, happens mainly in

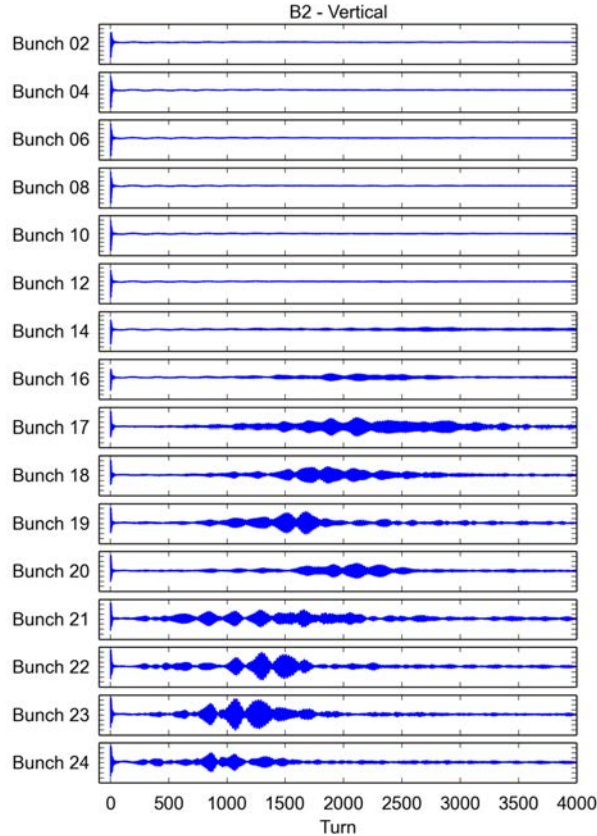


Fig. 12: Vertical position of selected bunches in a train of bunches over the first 4000 turns after injection. A transverse instability developing on the trailing bunches is clearly visible.

the vertical plane, if a large fraction of the driving electron cloud is concentrated in the dipoles, but it can equally affect the horizontal plane, if the driving electron cloud comes from drift sections or quadrupoles. In a machine like the LHC, which has 66% of its circumference covered by dipoles, the single-bunch instability will mainly affect the vertical plane, at least as long as the secondary electron yield of the beam screen of the dipoles is sufficiently high. The bunch-by-bunch position signal from the first 4000 turns after injection, as acquired from a beam position monitor for a train of 24 bunches, is given in Fig. 12 (every second bunch). It is clear that, while the first 12 bunches are stable, an unstable signal begins to appear after bunch 14 and the rise time of the instability tends to become shorter while moving to the tail of the train.

It must be noted here that this simple picture of the electron cloud single-bunch instability only applies for zero chromaticity. With non-zero chromaticity, the situation becomes more complex and the presence of an electron cloud can favour the onset of ‘classical’ head–tail instabilities in either plane, which can be damped with a classical transverse feedback system if the mode number is low enough to be handled by the system.

Even when the beam remains transversely stable, either because the integrated electron cloud density is low enough or thanks to stabilizing mechanisms (chromaticity, Landau damping, transverse feedback), its interaction with the electron cloud can drive incoherent effects, which slowly degrade the beam quality. These effects are usually caused by the fact that, even if the beam as a whole does not respond coherently to the electron cloud excitation, the single particles are still detuned by the additional transverse force coming from the electron cloud (usually focusing and strongly non-linear, but in general dependent on the detailed electron distribution) and their tunes can be individually pushed onto

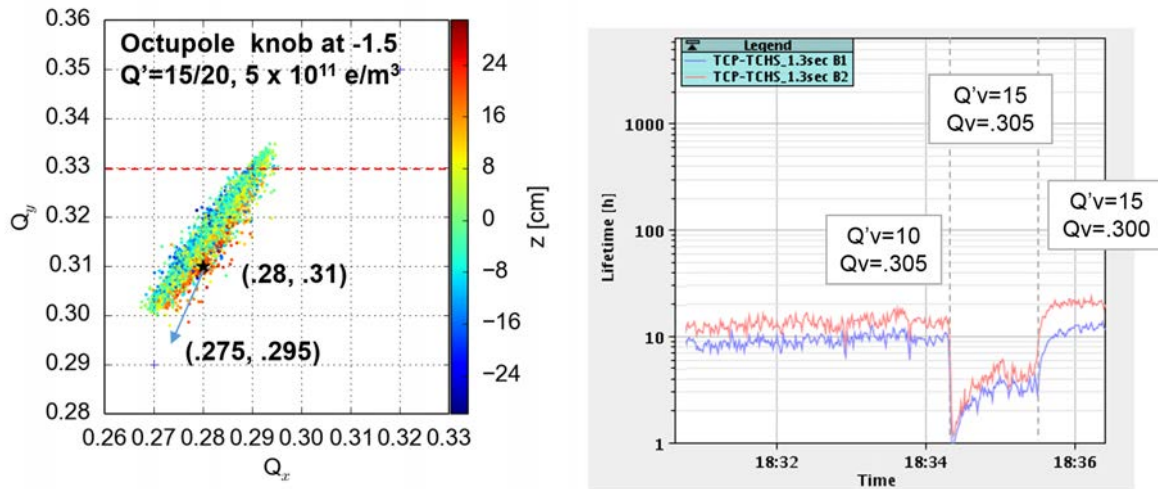


Fig. 13: Left-hand side: tune footprint at 450 GeV, as obtained from PyELOUD-PyHEADTAIL simulations. Right-hand side: beam lifetime measured with 25 ns beams in the LHC for different settings of vertical tune and chromaticity.

resonance lines with consequent growth of the particles' amplitudes. Therefore, the resulting tune spread from the electron cloud can be the origin of such phenomena as slow emittance blow-up or slow particle losses, which are particularly worrying in storage rings and colliders, where the aim is to store the beam in the ring for a very long time (several hours), while preserving beam quality, as much as possible, and limiting all types of unwanted beam loss. An example of an incoherent effect in the LHC is illustrated in Fig. 13. The left-hand plot shows the calculated tune spread of a single bunch in the LHC at injection energy (450 GeV), assuming the operational settings for chromaticity (15 units in the horizontal plane and 20 units in the vertical plane) and octupole currents (20 A), and in addition an electron cloud density of $5 \times 10^{11} \text{ m}^{-3}$ all around the machine dipoles. The nominal working point is (0.28, 0.31). The effect of the octupoles on the tune footprint is quite negligible compared with the one imprinted by chromaticity, while the electron cloud makes the tune spread asymmetrical around the nominal tunes by pushing the footprint towards higher tune values in the vertical plane. The visible consequence of the electron cloud contribution to the footprint is that some particles come to cross the third-order resonance. In this configuration, important losses are expected in the LHC, mainly affecting the bunches at the tails of the long injected trains. The right plot shows an experiment in the machine, in which a strong degradation of the beam lifetime was observed when increasing the vertical chromaticity from 10 to 15 units, which could be recovered (and even slightly improved) by moving the vertical tune down by 0.005.

3.2 Other effects

The presence of an electron cloud in a particle accelerator can be also revealed by the following observables.

- **Vacuum degradation:** The electron flux on the chamber's wall stimulates the desorption of gas molecules from the surface (dependent on the desorption yield of the wall for electron impingement), which results in an increased residual gas density in the beam chamber, and therefore in a pressure increase. This is obviously a local effect that can take place only in specific parts of the machine, which are prone to electron cloud formation as a result of their geometry or surface properties, or in extended machine sectors, if the beam chamber geometry and secondary electron yield are such as to support widespread electron cloud build-up. The pressure rise is associated with several deleterious effects, such as larger equipment irradiation, worse background in the

experimental areas, increased probability of breakdown in high-voltage devices like kickers or electrostatic septa, and impact on the beam lifetime [24].

- **Beam energy loss and heat load:** The electrons accelerated in the beam field subtract energy from the beam and also deposit a large fraction of this energy on the chamber's wall when they hit it and produce secondary electrons (usually it takes one electron with an energy of a few hundred electronvolts to produce one or more electrons with energies of a few electronvolts). Therefore, two different observables can be associated with this process:
 - first, if the amount of integrated electron cloud on the beam path is sufficiently large in the accelerator, then the total energy loss of a bunch due to the electron cloud over one turn can become significant. Since the lost energy must then be restored by the RF system, this can result in a measurable contribution to the stable (or synchronous) phase shift of the bunch in its RF bucket (beside the contributions coming from beam loading and the longitudinal impedance). This is a global measurement and provides information on the total amount of electron cloud present in the machine. Usually, this is assumed to be detectable if it is at least few tenths of a degree;
 - second, the energy deposited by the electrons on the chamber's wall heats it up and the additional heat load could be measured (either as an increase of the chamber wall's temperature or as an increased power required from the cooling system to keep the chamber at a desired temperature). This effect is only local and, while it is typically negligible in room temperature accelerator components, it can become a serious issue in devices operating at cryogenic temperatures, like the superconducting magnets of the LHC. Here, the heat load induced by the electron cloud can even reach the cooling capacity limit of the cryogenic system [25].
- **Impact on beam diagnostics:** The presence of an undesired electron flux at the frequency of the bunch spacing can be a source of spurious signals, and therefore malfunctions, on beam diagnostic devices, such as pick-ups (beam position monitors) and beam gas ionization chambers [26].

All these effects have been observed at the LHC and in its injector chain.

4 Mitigation strategies

In some cases, the accumulation of primary electrons alone inside the beam chamber of an accelerator can be the source of detrimental effects, even in the absence of beam-induced multipacting. Since this mainly happens for photoelectron production in bending or wiggler chambers of very-high-energy beams, an obvious mitigation technique would be to reduce the photoelectron production rate by either using surfaces with naturally low photoelectron yield or by guiding the photons into a region where the produced photoelectrons can then do no harm. When the electron cloud formation is mainly caused by secondary emission, it is necessary to find methods to reduce the effective secondary electron yield of the inner chamber walls in order to suppress or at least reduce the electron cloud build-up, and thereby limit its adverse effects. In either case, other viable options for mitigation could be:

- to alter the electron dynamics to avoid large fluxes of high-energy electrons towards the chamber walls. This can be achieved with electric fields (e.g., clearing electrodes) or magnetic fields (e.g., solenoids);
- not to suppress the electron cloud, merely alleviate its effects on the beam or on the devices that could be affected.

For machines like the KEKB photon factory, the LHC, and future circular colliders, the primary production of photoelectrons would be so high that the electron cloud could reach saturation within a few bunch passages, even without multipacting, if no countermeasures were taken. The solutions implemented in current machines are an antechamber (KEKB) or, for dipole fields, a sawtooth pattern impressed on the chamber wall (LHC). Weak solenoids of the order of 50 G are another possibility, which

was also successfully implemented at KEKB. The solenoids do not really reduce the photoemission, but they quickly loop the emitted photoelectrons back to the wall, thus mitigating the subsequent beam–electron interaction. For future circular colliders, different schemes are under study, based on photon absorbers or stoppers to intercept the photons at controlled locations and limit the associated photoelectron production, or on a novel design of the vacuum chamber with lateral slits shaped to trap the photons and subsequently shield the photoelectrons from the beam field. Electrons generated by beam loss at a collimator can be controlled by solenoids or clearing electrodes. For example, the SNS project has installed solenoids along the collimator straights.

When the electron cloud build-up is dominated by the process of secondary emission, the surface of the inner wall of the vacuum chamber needs to be treated such that its effective secondary electron yield is minimized, and ideally reduced to a value below 1. This can be achieved by either coating (i.e., changing the chemical properties of the exposed surface) or machining (i.e., changing the geometrical properties of the exposed surface). A well-established method to reduce multipacting in RF couplers is coating with TiN, a material that has been proven to condition to very low values of secondary electron yield. The thickness of the coating is of the order of a micrometre, which should not alter the resistive impedance seen by the beam.

A more favourable getter material made from TiZrV (a non-evaporable getter) was developed at CERN and has the advantage of pumping while having low secondary electron yield. This non-evaporable getter is characterized by greater structural stability than TiN, as well as a low activation temperature. The warm sections of the LHC, especially those around the experimental areas (about 20% of the circumference), have been coated with this material [27]. The non-evaporable getter coating has already been widely used at several synchrotron light sources around the world (both in insertion devices and for general coating of the vacuum chambers) to guarantee ultrahigh vacuum and improve the beam lifetime while reducing the probability of exciting fast beam ion instabilities.

In the last 10 years, impressive work has been done at CERN to develop a new type of coating with amorphous carbon, which does not require activation, has an intrinsically very low secondary electron yield and does not degrade with time [28]. This coating has been widely tested at the CERN Super Proton Synchrotron, where the suppression of the electron cloud was successfully proven in dedicated strip monitors, as well as in a few main bending units. In particular, an amorphous-carbon coated liner has remained installed in a strip monitor since 2007 and no electron cloud signal was ever measured in it, even after long technical stops and extensive machine venting. This confirms that the amorphous-carbon coating can preserve its low secondary electron yield even after being long exposed to air.

More recently, another type of procedure based on laser engineering of the surface (applicable, for example, to copper, stainless steel, and aluminium) has been proposed to reduce the effective secondary electron yield. The laser treatment, which imprints a surface topography made of organized microstructures, has the advantage of relatively easy application and possible retrofitting in existing machines [29]. In parallel with the research on coating and laser treating, several authors have also proposed a method to suppress multipacting by machining the wall surface to produce macroscopic grooves on it. These grooves essentially act as electron traps, as the electrons emitted by the surface are very likely to be re-absorbed quickly before they can be accelerated in the beam field. Much optimization work has been done to define the shape and the size of the grooves so as to obtain the best electron cloud suppression [30].

Finally, another way to reduce the secondary electron yield of the inner surface of an accelerator vacuum chamber is to rely on its conditioning with time, thanks to electron bombardment during beam operation with electron cloud. This technique is called ‘scrubbing’ and is based on the experimental observation that the secondary electron yield of a surface exposed to a continuous flux of high-energy electrons decreases with the deposited electron dose. While this decrease is usually very fast at the beginning for large values of the secondary electron yield, since scrubbing means physically removing the external layers of molecules and oxides present on the surface of the bare metal, it then tends to slow

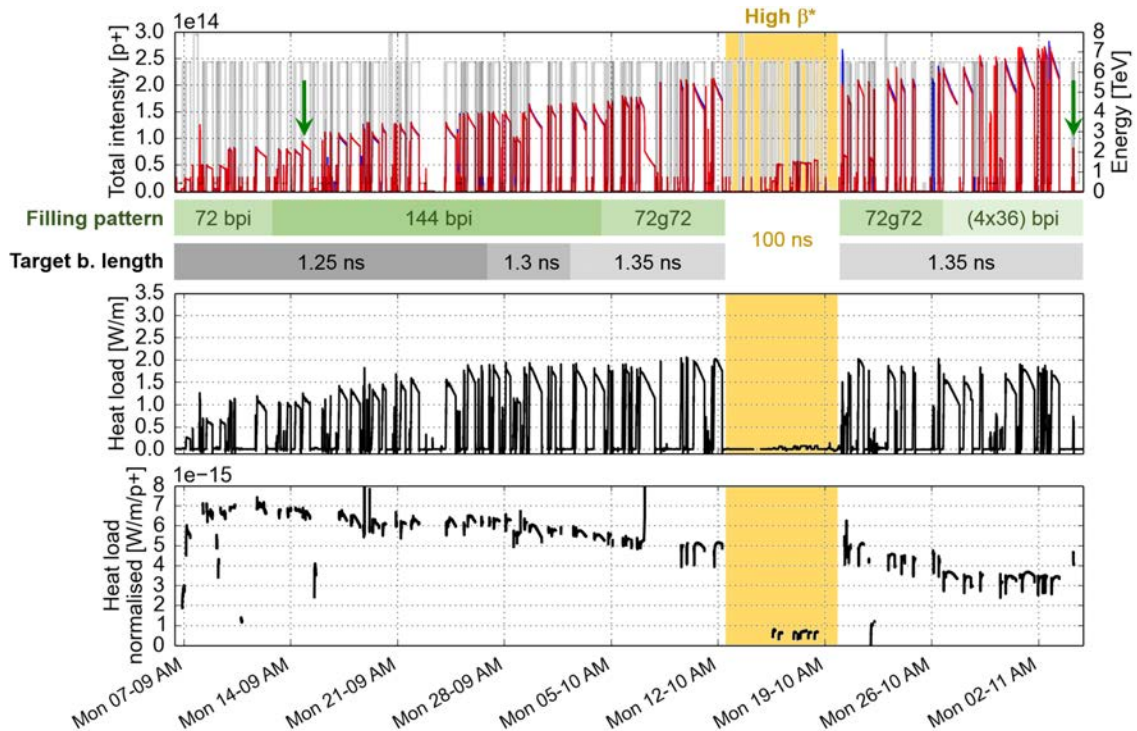


Fig. 14: Evolution of (top) beam intensity, (middle) average heat load in the arc magnets, and (bottom) heat load normalized to the beam intensity during the intensity ramp-up, with 25 ns beams

down exponentially and eventually requires enormous doses to make tiny steps in the region of secondary electron yields below 1.3–1.4.

Scrubbing has been widely used at CERN for the Super Proton Synchrotron and LHC, both of which have reached nominal operation with 25 ns beams thanks to extended scrubbing runs. In the case of the LHC, an important part of the scrubbing process has been carried out not only through dedicated scrubbing periods, necessary nevertheless to prepare the machine to operate with 25 ns beams, but also through physics stores with 25 ns beams. Assuming the heat load in the cold arcs to be a measure of the amount of electron cloud present in the machine, Fig. 14 displays the evolution of this quantity over two months during the 2015 run, when increasing numbers of bunches were injected into the LHC and brought to collision at 6.5 TeV. The scrubbing of the surface of the beam screen in the arcs is visible as the decrease of the heat load normalized to the total beam current, which has taken place with a time constant of weeks and has led to about half the value over the full two months' period. For completeness, it must be highlighted here that the decrease of the normalized heat load is not fully ascribable to surface scrubbing, but was also aided by relaxing the filling pattern into the LHC (moving from trains of 72 bunches to trains of 36 bunches) and increasing the bunch length at top energy (as shown in the plot of 'filling pattern' and the 'target beam length' strips). These additional electron cloud mitigating measures were necessary to increase the number of bunches injected into LHC, while keeping the produced heat load in the arcs within the cooling capacity of the cryogenic system.

Multipacting may also be suppressed by solenoids, though one should pay attention to the possibility of cyclotron resonances (i.e., conditions for which the cyclotron period of the electrons in the solenoid field is a multiple of the bunch spacing). Electric clearing fields are also an efficient cure in simulations. They were already used to cure electron–proton instabilities for the coasting proton beams in the CERN ISR during the early 1970s. At the SNS, operating with long proton bunches, all beam position monitors can be biased with a clearing voltage of 1 kV. To be effective for the multipacting experienced by short bunches with close spacing, the clearing electrodes must be mounted all around

the ring at close distances and voltages of the order of 1 kV are probably required. The impedance introduced by many such devices could be an obvious showstopper. However, a continuous long wire on an insulating support would not necessarily exhibit a prohibitively large impedance. Other options for a practical implementation of electric clearing fields might involve using ‘stealth’ electrodes, or splitting the beam pipe into top and bottom halves, isolated from each other and held at different potentials. Biasing the two jaws of a collimator against each other is a similar idea.

Proper tailoring of the bunch filling patterns (bunch spacing, bunch trains, and bunch charges) is yet another way of achieving an acceptable electron density. The application of this technique can be two-fold. On the one hand, the arrangement of the bunches in a train can be such as to minimize the electron cloud build-up and allow an electron cloud free operation of the accelerator. In particular, a larger bunch spacing can help, or gaps within trains can reduce the electron cloud density and reset the cloud, at least partly. However, this usually comes at the expense of the total amount of beam intensity that can be accelerated in the machine, as the full potential of the available free buckets is not exploited. Examples here include mini-trains in the PEP-II, the actual bunch spacings chosen for the PEP-II and KEKB operation, which are two or three times the design spacing, the 150–75–50 ns beam configuration used until 2012 in the LHC, and finally the so-called 8b + 4e configuration for 25 ns proposed for the LHC, in which long trains of 25 ns spaced bunches are replaced with trains exhibiting gaps of four empty buckets for every eight full buckets [7]. On the other hand, special beam configurations can be put in place, with the goal of increasing as much as possible the electron cloud formation and accelerate the scrubbing process. A typical example of this approach is the use of ‘doublet’ beams in the Super Proton Synchrotron and LHC, i.e., beams made of 5 ns spaced bunch pairs separated from each other by 25 ns. These beams were expected, and proved, to produce a large electron cloud in both the Super Proton Synchrotron and LHC, offering the potential of possibly scrubbing the wall surfaces to secondary electron yields below the electron cloud build-up thresholds for the nominal 25 ns beams [7].

Acknowledgements

We would like to thank G. Arduini, H. Bartosik, K. Li, L. Mether, A. Romano, M. Schenk, F. Zimmermann and many others for their invaluable help in electron cloud studies at the CERN accelerator complex over the years.

References

- [1] W. Fischer *et al.*, *Phys. Rev. Spec. Top. Accel. Beams* **11** (2008) 041002. <https://doi.org/10.1103/PhysRevSTAB.11.041002>
- [2] H. Fukuma, in Proc. E-CLOUD12: Joint INFN-CERN-EuCARD-AccNet Workshop on Electron-Cloud Effects, La Biodola, Isola d’Elba, Italy, edited by R. Cimino, G. Rumolo, F. Zimmermann, CERN-2013-002 (CERN, Geneva, 2013), pp. 27-30. <https://doi.org/10.5170/CERN-2013-002.27>
- [3] M. Zobov *et al.*, in Proc. E-CLOUD12: Joint INFN-CERN-EuCARD-AccNet Workshop on Electron-Cloud Effects, La Biodola, Isola d’Elba, Italy, edited by R. Cimino, G. Rumolo, F. Zimmermann, CERN-2013-002 (CERN, Geneva, 2013), pp. 259-265. <https://doi.org/10.5170/CERN-2013-002.259>
- [4] G. Rumolo *et al.*, Electron cloud observation in the LHC, Proc. IPAC11 Int. Particle Accelerator Conf., San Sebastian, Spain, edited by Petit-Jean-Genaz *et al.*, 2011, p. 2682.
- [5] G. Rumolo *et al.*, Electron cloud effects in the LHC in 2011, Proc. Evian 2011 LHC Beam Operation Workshop, Evian, France, edited by B. Goddard and S. Dubourg, CERN-ATS-2012-083, p.165, 2011.
- [6] G. Iadarola *et al.*, Electron cloud effects in 2012 in the LHC, Proc. Evian 2012 LHC Beam Operation Workshop, Evian, France, edited by B. Goddard and S. Dubourg, CERN-ATS-2013-045, p. 119, 2012.

- [7] G. Iadarola *et al.*, Performance limitations from electron cloud in 2015, Proc. Evian 2015 LHC Beam Operation Workshop, Evian, France, edited by S. Dubourg and B. Goddard, CERN-ATS-2015-376, p. 101, 2015.
- [8] G. Rumolo *et al.*, *Phys. Rev. Spec. Top. Accel. Beams* **4** (2001) 012801.
<https://doi.org/10.1103/PhysRevSTAB.4.012801>
- [9] B. Henrist *et al.*, in Mini Workshop on Electron Cloud Simulations for Proton and Positron Beams, 15–18 April 2002, CERN, Geneva, Switzerland, edited by G. Rumolo and F. Zimmermann, CERN-2002-001 (CERN, Geneva, 2002), pp. 75-78. <https://doi.org/10.5170/CERN-2002-001.75>
- [10] V. Baglin *et al.*, A summary of main experimental results concerning the secondary electron emission of copper. LHC Project Report 472 (2002).
- [11] R. Cimino *et al.*, *Phys. Rev. Lett.* **93** (2004) 014801.
<https://doi.org/10.1103/PhysRevLett.93.014801>
- [12] R. Cimino and I.R. Collins. *Appl. Surf. Sci.* **235** (2004) 231.
<https://doi.org/10.1016/j.apsusc.2004.05.270>
- [13] A. Kuzucan *et al.*, Secondary electron yield on cryogenic surfaces as a function of physisorbed gases, Proc. IPAC11 Int. Particle Accelerator Conf., San Sebastian, Spain, edited by Petit-Jean-Genaz *et al.*, p. 1575, 2011.
- [14] G. Iadarola and G. Rumolo, in Proc. E-CLOUD12: Joint INFN-CERN-EuCARD-AccNet Workshop on Electron-Cloud Effects, La Biodola, Isola d'Elba, Italy, edited by R. Cimino, G. Rumolo, F. Zimmermann, CERN-2013-002 (CERN, Geneva, 2013), pp. 189-194. <https://doi.org/10.5170/CERN-2013-002.189>
- [15] D. Halliday *et al.*, *Fundamentals of Physics* (John Wiley, New York, 2010).
- [16] R.J. Macek *et al.*, *Phys. Rev. Spec. Top. Accel. Beams* **11** (2008) 010101.
<https://doi.org/10.1103/PhysRevSTAB.11.010101>
- [17] F. Zimmermann, Electron cloud studies for the low energy ring of KEKB, CERN-SL-Note-2000-004, 2000.
- [18] G. Arduini *et al.*, The LHC proton beam in the CERN SPS: an update, 20th IEEE Particle Accelerator Conf., Portland, OR, USA, 2003. <https://doi.org/10.1109/pac.2003.1288647>
- [19] R. Cappi *et al.*, *Phys. Rev. Spec. Top. Accel. Beams* **5** (2002) 094401.
<https://doi.org/10.1103/PhysRevSTAB.5.094401>
- [20] H. Bartosik *et al.*, in Proc. E-CLOUD12: Joint INFN-CERN-EuCARD-AccNet Workshop on Electron-Cloud Effects, La Biodola, Isola d'Elba, Italy, edited by R. Cimino, G. Rumolo, F. Zimmermann, CERN-2013-002 (CERN, Geneva, 2013), pp. 211-217. <https://doi.org/10.5170/CERN-2013-002.211>
- [21] A.W. Chao, *Physics of Collective Beam Instabilities in High Energy Accelerators* (Wiley, New York, 1993).
- [22] K. Li and G. Rumolo, Review of beam instabilities in the presence of electron clouds in the LHC, Proc. IPAC11 Int. Particle Accelerator Conf., San Sebastian, Spain, edited by Petit-Jean-Genaz *et al.*, p. 760, 2011.
- [23] K. Li *et al.*, LHC injection instabilities, Presentation at 2-day internal review of LHC performance limitations during run I, 25–26 Sept. 2013, CERN, 2013.
- [24] G. Bregliozzi *et al.*, Vacuum pressure observations during 2011 proton run, Proc. Evian 2011 LHC Beam Operation Workshop, Evian, France, edited by B. Goddard and S. Dubourg, CERN-ATS-2013-083, p. 177, 2011.
- [25] L. Taviani, Performance limitations of the LHC cryogenics: 2012 review and 2015 outlook, Proc. Evian 2012 LHC Beam Operation Workshop, Evian, France, edited by B. Goddard and S. Dubourg, CERN-ATS-2013-045, p. 129, 2012.

- [26] W. Höfle, Observations of the electron cloud effect on pick-up signals in the SPS. 10th Workshop on LEP-SPS Performance, Chamonix, France, edited by P. Le Roux, J. Poole and T. Truchet, CERN-SL-2000-007-DI, p. 102, 2000.
- [27] O. Bruning *et al.*, *LHC Design Report* (CERN, Geneva, 2004).
- [28] C. Yin Vallgren *et al.*, *Phys. Rev. Spec. Top. Accel. Beams* **14** (2011) 071001.
<https://doi.org/10.1103/PhysRevSTAB.14.071001>
- [29] R. Valizadeh *et al.*, *Appl. Phys. Lett.* **105** (2014) 231605. <https://doi.org/10.1063/1.4902993>
- [30] G. Stupakov and M. Pivi, in Proc. 31st Advanced ICFA Beam Dynamics Workshop on Electron-Cloud Effects, 19–23 April 2004, Napa, CA, USA, CERN-2005-001 (CERN, Geneva, 2005), pp. 139-141. <https://doi.org/10.5170/CERN-2005-001.139>